Article

On the Correlation of Cymbals' Vibrational Behavior and Manufacturing Processes

Spyros Brezas *, Evaggelos Kaselouris, Yannis Orphanos, Makis Bakarezos, Nektarios A. Papadogiannis and Vasilis Dimitriou

Physical Acoustics and Optoacoustics Laboratory, School of Music and Optoacoustic Technologies, Hellenic Mediterranean University, Perivolia, 71433 Rethymnon, Greece; vagfem@hmu.gr (E.K.); yorphanos@hmu.gr (Y.O.); bakarezos@hmu.gr (M.B.); npapadogiannis@hmu.gr (N.A.P.); dimvasi@hmu.gr (V.D.)
* Correspondence: sbrezas@hmu.gr

Abstract: The complex frequency domain assurance criterion is here applied for the comparison of a pristine to an altered state of a vibrating system. The criterion was originally proposed for the detection of defects in vibrating structures, while in later research studies it has been successfully used in musical acoustics. In this paper, we evaluate the differences in the vibrational behavior of finished and non-finished cymbals by adopting the proposed correlation criterion. Since idiophones are playable and produce sounds after any manufacturing process, the methodology presented correlates the vibrational state of a cymbal, at any stage of manufacturing, to a reference pristine cymbal. The evaluation of the cymbals is performed by the comparison of finished cymbals with semi-finished and blank 8-inch cymbals of the same material. The correlation criterion is applied to the vibrational measurements of blank, semi-finished, and finished B8 and B20 cymbals. Additionally, commercially available finished cymbals of the same material and geometrical characteristics are introduced in this correlation study. The measuring methodology and the vibration symmetry are discussed, and valuable results and conclusions are presented. The proposed methodology highlights the influence of the manufacturing processes of forming, hammering, and finishing on the vibrational behavior of cymbals, offering manufacturers and drummers a quantifiable criterion for evaluating cymbals' vibroacoustic performance. Representative evaluations of blanks, semi-finished, and finished cymbals demonstrate the capability of the correlation criterion to monitor, identify, and visualize the vibrational state of any cymbal compared to a pristine reference. This enables the development of a novel methodology for both manufacturers and musicians.

Keywords: cymbal manufacturing; cymbal vibrational behavior; complex frequency domain assurance criterion

1. Introduction

The vibration of percussion instruments has been the topic of interest for many studies in the field of musical acoustics. Cymbals are among the most popular percussion instruments and have been studied by various methods [1–3]. The weight, size, shape of the bell, and the material of construction all affect the sound of the cymbal, while an intriguing aspect is their nonlinear vibrational behavior, which has been the focus of numerous studies [1–3]. A cymbal is a struck idiophone that belongs to the same category of percussion instruments as gongs, chimes, sound plates, and triangles. These instruments are typically played by striking them with mallets or sticks [3]. Cymbals and gongs [4]

follow similarly complex manufacturing stages, while chimes [5], sound plates [6], and triangles [7] are relatively simpler to construct.

Cymbals are made from alloys [8], which are primarily based on copper combined mainly with tin (bronze), nickel (nickel silver), and zinc (brass). Other materials, such as silver, gold, and phosphorus are also used but in much smaller proportions. Cymbals are typically crafted from cast ingots, which are shaped into discs, which in turn are hot-forged and lead to the formation of roughly shaped cymbals. These roughly shaped cymbals are rolled and formed into a dome shape by cupping and spinforming, and are generally called blanks. Blanks are hardened by hammering to semi-finished cymbals, which are finished by lathing, leading to thickness reduction [8]. Finishing may include additional thickness adjustments and polishing. Hammering is a crucial step since it creates tension and stress within the material. Large hammer marks cause discontinuities in the material that are similar in scale to the wavelength of cymbal vibrations, thereby influencing the sound [3].

In the literature, the presence of mixed modes in cymbals was investigated in [9]. Aiming to synthesize the sound of cymbals, a model was proposed [10] using a modal approach. This study also highlighted the importance of incorporating damping in such models. In another study on sound synthesis, the importance of the geometrical properties of cymbals was discussed [11]. A model focusing on thickness variations in cymbals was also presented in [12]. The vibrational behavior of cymbals was also studied, using the finite element method (FEM) and sound synthesis [13]. This approach was further enhanced by incorporating vibration measurements and accounting for geometry variations in cymbals [14]. The emitted sound from cymbals was also the topic of a study that highlighted the importance of the instrument's geometry [15], while vibroacoustic numerical simulations of motion-driven cymbal–drumstick interactions were shown in [16]. Furthermore, the effect of the hammering process on the emitted sound was studied via experiments and simulations in [17].

Based on the aforementioned studies, the majority of research focuses on commercially available finished cymbals, which offer clear, observable acoustic outcomes that researchers can measure and analyze, making them ideal for studies involving sound characteristics, resonance, and tonal quality. In contrast, less extensive research has explored the manufacturing process to investigate how, and to what extent, each stage of manufacturing affects the resulting sound. To the authors' knowledge, one comprehensive study has examined the correlation between the emitted sound and the distribution of residual stress and strain in cymbals [18]. Since idiophones do not need to be processed to a particular finished state to be played, the study of raw cymbals during their manufacturing is demanded to trace how changes in shape, thickness, and material composition evolve and affect sound quality throughout the production process. Well-established brands are nowadays providing commercial unfinished cymbals [19,20] to meet the needs of the music market. Studying unfinalized cymbals provides deeper insights into how different alloys, microstructures, and treatments (e.g., annealing) impact cymbal quality, far beyond what is typically visible in finished products.

In this study, we adopt a correlation criterion and a related index to track and identify changes in the vibration behavior (in terms of frequency response) of blank, semi-finished, and finished cymbals during their manufacturing. This methodology is proposed for evaluating and controlling the modifications in the cymbals' vibration behavior during production, up to the finished commercial cymbals. Therefore, commercially available finished cymbals are also introduced in our study. The innovation of this work lies in the novel application of the complex frequency domain assurance criterion (CFDAC) [21,22] to systematically analyze and quantify the vibrational behavior of cymbals across various states of manufacturing. By applying the CFDAC to compare blank, semi-finished,

and finished cymbals, this study provides a robust, data-driven understanding of how manufacturing processes—such as forming, hammering, and finishing—affect vibrational properties. The ability to identify vibrational changes at each stage is of critical importance in cymbal design and performance. This bridges a gap between craftsmanship and measurable acoustical science and provides a quantifiable criterion for cymbals' vibroacoustic performance, regardless of the manufacturing state. The proposed methodology also provides manufacturers with a new technological tool to assess and refine their production processes, ensuring consistency and maximizing the acoustic quality of their products, thereby revealing new sound possibilities that could be refined into new commercially viable products.

2. Theoretical Background

2.1. Complex Frequency Domain Assurance Criterion

The frequency response function (FRF) of a system $h_{ij}(\omega)$ relates a single force $f_j(\omega)$ excitation applied to point j to a response $x_i(\omega)$ detected at point i by $x_i(\omega) = h_{ij}(\omega)f_j(\omega)$. All FRFs contain information about the dynamic characteristics of a system, which in matrix notation can be expressed as $H(\omega) = X(\omega)F^{-1}(\omega)$, where $H(\omega)$ is the matrix containing all FRFs, $X(\omega)$ is the matrix containing all responses, and $F(\omega)$ the matrix containing all applied forces. To identify damage in a system, Perez et al. [21,22] proposed the complex frequency domain assurance criterion (CFDAC). The use of the CFDAC, a spectral domain indicator, offers advantages compared to modal, spatial, or temporal analysis. The CFDAC is calculated following a convenient condensing procedure that avoids information loss by applying the Fourier transform. It requires simplified post-processing and provides enhanced sensitivity to reinforcement or degradation [23]. This means that variations in the dynamic response of the structure, resulting from alterations, can be detected. The detection of such alterations becomes feasible by comparing two states.

In the case of comparing a pristine state (denoted as *p*) with an altered state (denoted as *a*), after acquiring the response of the system at *N* points, the CFDAC is defined for each frequency pair $\left(\omega_f, \omega_g\right)$ as follows:

$$\text{CFDAC}_{fg} = \frac{\left[\sum_{i=1}^{N}\sum_{j=1}^{N} h_{ij}^{(p)}\left(\omega_f\right)h_{ij}^{(a)}(\omega_g)\right]^2}{\left[\sum_{i=1}^{N}\sum_{j=1}^{N} h_{ij}^{(p)}\left(\omega_f\right)h_{ij}^{*(p)}\left(\omega_f\right)\right]\left[\sum_{i=1}^{N}\sum_{j=1}^{N} h_{ij}^{(a)}(\omega_g)h_{ij}^{*(a)}(\omega_g)\right]} \in \mathbb{C} \quad (1)$$

where $h^{(p)}(\omega)$ is the set of FRFs for the pristine state, $h^{(a)}(\omega)$ is the set of FRFs for the altered state, ω_f and ω_g denote the frequency (FFT line indices) of the pristine and altered states, respectively, *i* is the index for the location of the response point, *j* is the index for the excitation point, and * denotes the complex conjugate. For mathematical consistency, it must be ensured that all FRFs have the same amount of frequency lines ($N_f = N_g$) and resolution. Hence, CFDAC_{fg} is an $N_f \times N_f$ array. The criterion is an indicator of the covariance between the two sets of FRFs $h^{(p)}(\omega)$ and $h^{(a)}(\omega)$, which are compared for each pair of spectral lines. The values of CFDAC_{fg} are confined to the $[-1, 1]$, $[-j, j]$ region of the complex plane. If the same set of FRFs is used for both the pristine and altered states, then the CFDAC_{fg} array exhibits a perfect diagonal structure. The real part of the CFDAC_{fg} shows the correlation of the resonant peaks with their adjacent frequencies, whereas the imaginary part shows the correlation at the central frequencies of the lobes. Recently, the CFDAC was successfully extended to musical acoustics in terms of comparing results from simulations, measurements, and parts of musical instruments during additive manufacturing [23–25].

2.2. Spectral Correlation Index

Concerning cymbals, the CFDAC can be used to monitor and classify unfinished cymbals during manufacturing stages based on alterations in the CFDAC pattern. This requires two CFDACs to be compared. The first CFDAC is the correlation of the FRFs of a cymbal, C1 (denoted by $\text{CFDAC}_{h^{(C1)},h^{(C1)}}$). The second CFDAC is the correlation of the C1 FRFs to a set of FRFs of another cymbal, C2 (denoted by $\text{CFDAC}_{h^{(C1)},h^{(C2)}}$). For assessing the similarity between $\text{CFDAC}_{h^{(C1)},h^{(C1)}}$ and $\text{CFDAC}_{h^{(C1)},h^{(C2)}}$, quantitative indicators are required, which are derived from image structure similarity indicators. The Pearson correlation coefficient (PCC) is used to quantify the degree of similarity of the compared CFDACs [26]. It is described by

$$\text{PCC}_{A,B} = \frac{\sum_{f=1}^{N_f} \sum_{g=1}^{N_g} A_{fg} B_{fg} - N_f N_g \overline{AB}}{\left(N_f N_g - 1\right) \sigma_A \sigma_B} \tag{2}$$

where N_f and N_g are the FRFs' frequency lines, as stated above ($N_f = N_g$). The terms A_{fg} and B_{fg} correspond to $\text{CFDAC}_{h^{(C1)},h^{(C1)}}$ and $\text{CFDAC}_{h^{(C1)},h^{(C2)}}$, respectively. As it may be assumed, in Equation (2), either the real parts, i.e., $A_{fg}^{\text{Re}} = \text{Re}\left\{\text{CFDAC}_{h^{(C1)},h^{(C1)}}\right\}$ and $B_{fg}^{\text{Re}} = \text{Re}\left\{\text{CFDAC}_{h^{(C1)},h^{(C2)}}\right\}$, or the imaginary parts, i.e., $A_{fg}^{\text{Im}} = \text{Im}\left\{\text{CFDAC}_{h^{(C1)},h^{(C1)}}\right\}$ and $B_{fg}^{\text{Im}} = \text{Im}\left\{\text{CFDAC}_{h^{(C1)},h^{(C2)}}\right\}$, can be used. It must be noted that for the calculation of PCC, the CFDAC matrices must be reshaped to $1 \times N_f N_g$ arrays.

The term $\overline{A}$ corresponds to mean value of the array according to

$$\overline{A} = \frac{1}{N_f N_g} \sum_{f=1}^{N_f} \sum_{g=1}^{N_g} A_{fg} \tag{3}$$

The same equation is used for the term $\overline{B}$.

The term σ_A corresponds to the standard deviation of the array according to

$$\sigma_A = \sqrt{\frac{1}{N_f N_g - 1} \sum_{f=1}^{N_f} \sum_{g=1}^{N_g} \left(A_{fg} - \overline{A}\right)^2} \tag{4}$$

The same equation can be used for the term σ_B.

The PCC values are real and fall within the range of $[-1, 1]$. A value of 0 indicates no correlation, 1 represents perfect linear correlation, and -1 indicates an inverse or negative correlation. However, the latter case, which represents inverse frequency correlation, is not applicable to the present study. Therefore, the range is modified to $[0, 1]$.

The spectral correlation index (SCI) is determined as

$$\text{SCI}_{A,B} = 1 - |\text{PCC}_{A,B}| \in \mathbb{R} \tag{5}$$

This transformation was adopted by Perez et al. [26] for convenience, as they consider the value 0 to be a better descriptor for fully correlated states and 1 for completely uncorrelated states. Additionally, the SCI condenses all the information from the CFDAC matrices into a single value. Furthermore, the SCI can be calculated either from the real or the imaginary parts of the considered CFDACs, as described in [26].

3. Experimental Measurement Setup

Nineteen 8-inch cymbals made of MS63, B8, and B20 are studied in this work. A group of five B8 blanks, noted as B8-1, B8-2, B8-3, B8-4, and B8-5, and a group of four blank B20 cymbals, noted as B20-41, B20-42, B20-43, and B20-44, are included. A group of five B20

semi-finished hammered cymbals are also studied, noted as B20-51, B20-52, B20-53, B20-54, and B20-55. Additionally, five finished/commercial cymbals—an MS63, a B8 (noted as B8-0), and three B20s (noted as B20-1, B20-2, and B20-3)—are introduced in this study.

The cymbals are presented and described in Table 1. It is noticed that the finished/commercial cymbals are of similar curvature and mass, while the MS63 cymbal stands out as having the greatest mass and curvature of them all. For the cymbal groups, the mass values in Table 1 correspond to the mean value for each group. Since the proposed methodology may be applied to any type of cymbal at any manufacturing state, the brand names of the manufacturers have been blurred.

Table 1. Characteristics of the 8-inch cymbals studied.

Alloy	Quantity	Index	Diameter (in)	Mass (g)	Manufacturing Stage			Cymbal	
					Blank	Semi-Finished	Finished/Commercial	Front View	Side View
MS63	1	MS63	8	380			✓		
B8	1	B8-0	8	195			✓		
B8	5	B8-1,2,3,4,5	8	222	✓				
B20	1	B20-1	8	151			✓		
B20	1	B20-2	8	150			✓		
B20	1	B20-3	8	157			✓		
B20	4	B20-41,42,43,44	8	241	✓				
B20	5	B20-51,52,53,54,55	8	247		✓			

A miniature impact hammer (Model 086E80, PCB, Depew, NY, USA) [27] and a miniature accelerometer (Model TLD352A56, PCB, Depew, NY, USA) [28] were used to excite each cymbal and detect the response. Since acceleration is the required kinematic quantity, the FRF is expressed in terms of accelerance. The auto- and cross-spectra of the signals are used for the calculation of the estimator H_2 $\left((\text{m/s}^2)\,/\,\text{N} \right)$, which is described by

$$H_2(\omega) = \frac{G_{aa}(\omega)}{G_{Fa}(\omega)} \tag{6}$$

where $G_{aa}(\omega)$ is the auto-spectrum of the acceleration and $G_{Fa}(\omega)$ is the cross-spectrum of the force and the acceleration [29]. The signals were recorded and further processed by a real-time multi-analyzer (Model OR34, OROS, Montbonnot-Saint-Martin, France). According to Perez et al.'s analysis [26], the sampling frequency is set to 8.192 kHz, providing 6401 FFT lines with 0.5 Hz frequency resolution up to 3.2 kHz. The roving excitation method was used on a grid of 144 measurement points on each cymbal. This number of points preserves the stability of calculations, as explained in detail in the following section (Section 4.1). Each point is excited 5 times for averaging. The grid consists of 16 radii, each with 9 points spaced 1 cm apart, as shown in Figure 1. The accelerometer was attached to the cymbal using wax and positioned at a point where a drummer typically strikes with a drumstick. A torque gauge (Model BTG, Tohnichi, Tokyo, Japan) was used to ensure repeatable screw tightening.
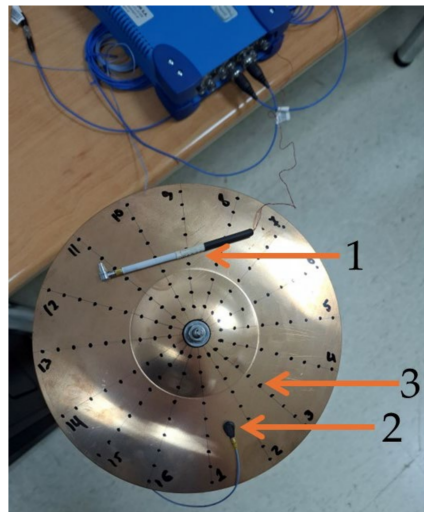
Figure 1. Measurement setup. Impact hammer (1), accelerometer (2), and measurement grid of 144 points (3) on the B8-1 cymbal.

To preserve the stability criterion of the CFDAC calculations, the number of measurement points is initially determined (144 in our case, as explained in detail in Section 4.1). An axis-symmetric grid of the 144 uniformly distributed points is developed on the cymbal under study, as presented in Figure 1. The roving excitation method is applied to the grid of the measurement points on each cymbal. The FRFs of the cymbals under consideration are measured by the impact hammer and accelerometer. Then, the CFDAC of the required FRF set is calculated. The CFDACs are further used for the derivation of the SCI. The flowchart of the aforementioned methodology is presented in Figure 2.
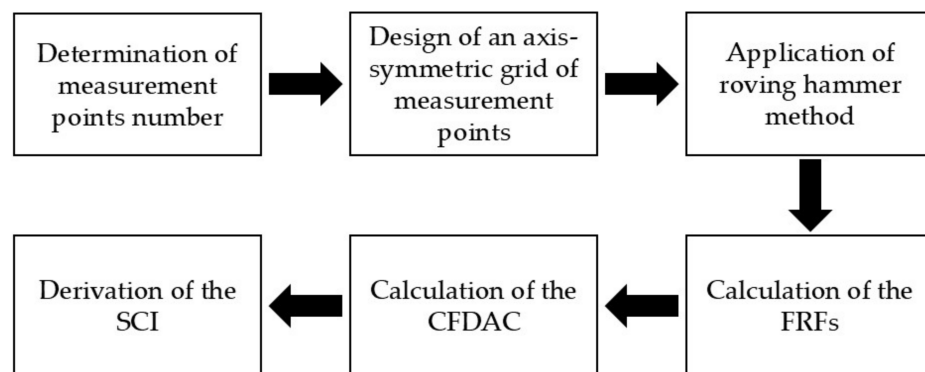
Figure 2. Flowchart of the proposed methodology application for measurements and calculations.

4. Results

4.1. Stability Calculations

The information derived from the CFDAC, and subsequently the SCI, is strongly related to frequency resolution [26]. In the present study, the effect of the number of measurement points, which determines the number of rows of the CFDAC matrix, is discussed. The SCI was calculated for various numbers of measurement points, namely 14, 28, 42, 56, 70, 84, 98, 112, 124, and 144. For the calculations, the measurement data of the B8-0, B8-1, B8-2, B8-3, B8-4, and B8-5 cymbals were used. The SCI was derived using the CFDAC pairs between B8-0 and the other cymbals (e.g., $\mathrm{CFDAC}_{h^{(B8\text{-}0)},h^{(B8\text{-}0)}}$ and $\mathrm{CFDAC}_{h^{(B8\text{-}0)},h^{(B8\text{-}1)}}$). Each measurement number corresponds to an FRF. The FRFs for this analysis were randomly selected. For each point value (e.g., 14), the random selection was performed five times, providing five different sets of FRFs to be considered. Each set of FRFs was used for the calculations between the B8-0 cymbals and one of the remaining cymbals (e.g., the first set of FRFs was used for the $\mathrm{CFDAC}_{h^{(B8\text{-}0)},h^{(B8\text{-}0)}}$ and $\mathrm{CFDAC}_{h^{(B8\text{-}0)},h^{(B8\text{-}1)}}$ comparison). Figure 3 shows the SCI values calculated using both the real and imaginary values of the CFDACs.
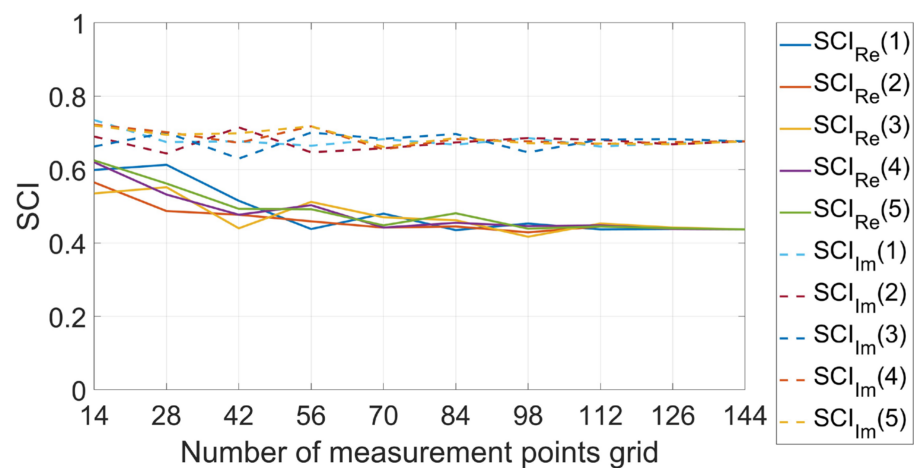
Figure 3. SCI values vs. the numbers of measurement points from 14 to 144 by a step of 14, tested for the stability of the calculations, based on the real (solid lines) and on the imaginary (dashed lines) values of CFDACs.

Figure 3 shows the convergence of the SCI values when the 144 measurement points are considered, since small variations are noticed even if a grid of 126 points is used, prescribing the use of all measurement points for the subsequent calculations presented in the paper. It should be noted that the SCI values based on the imaginary parts of the CFDACs (SCI_{Im}) are greater than the values based on the real parts (SCI_{Re}), in agreement with the findings originally presented and described in [26]. It is assumed that the correlation of the resonance frequencies at the centers of the lobes contribute to the higher values of the SCI_{Im}.

4.2. Correlation Between Blanks

The highest correlation values are expected to occur by comparing similar cymbals. This is the case for the blank B8 cymbals (B8-1, B8-2, B8-3, B8-4, and B8-5) due to their similar mass and shape. The CFDAC was calculated by considering B8-1 to be the reference (pristine) cymbal, providing $\mathrm{CFDAC}_{h^{(B8\text{-}1)},h^{(B8\text{-}1)}}$, $\mathrm{CFDAC}_{h^{(B8\text{-}1)},h^{(B8\text{-}2)}}$, $\mathrm{CFDAC}_{h^{(B8\text{-}1)},h^{(B8\text{-}3)}}$, $\mathrm{CFDAC}_{h^{(B8\text{-}1)},h^{(B8\text{-}4)}}$, and $\mathrm{CFDAC}_{h^{(B8\text{-}1)},h^{(B8\text{-}5)}}$. The CFDACs were used for the calculation of the SCI. Figure 4 shows the absolute values of the real (Re{ }) and imaginary (Im{ }) parts of the CFDACs, which are confined within the range of [0, 1], and the same holds for the forthcoming plots in the manuscript. Regarding the relationship

between the CFDAC matrix data and the plot, it should be noted that in the plots, the rows increase from bottom to top. Additionally, for all CFDAC plots in the article, the horizontal axis corresponds to the first set of FRFs and the vertical to the second set.
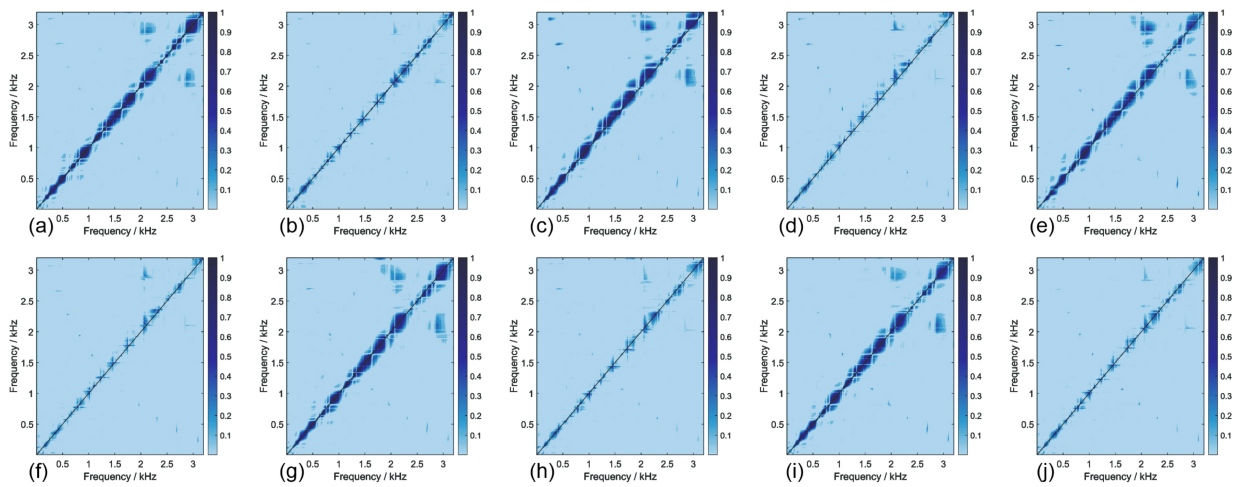
Figure 4. CFDACs between FRFs of B8-1 and B8-1, B8-2, B8-3, B8-4, and B8-5 cymbals. **(a)** $\mathrm{Re}\left\{\mathrm{CFDAC}_{h^{(\mathrm{B8\text{-}1})},h^{(\mathrm{B8\text{-}1})}}\right\}$, **(b)** $\mathrm{Im}\left\{\mathrm{CFDAC}_{h^{(\mathrm{B8\text{-}1})},h^{(\mathrm{B8\text{-}1})}}\right\}$, **(c)** $\mathrm{Re}\left\{\mathrm{CFDAC}_{h^{(\mathrm{B8\text{-}1})},h^{(\mathrm{B8\text{-}2})}}\right\}$, **(d)** $\mathrm{Im}\left\{\mathrm{CFDAC}_{h^{(\mathrm{B8\text{-}1})},h^{(\mathrm{B8\text{-}2})}}\right\}$, **(e)** $\mathrm{Re}\left\{\mathrm{CFDAC}_{h^{(\mathrm{B8\text{-}1})},h^{(\mathrm{B8\text{-}3})}}\right\}$, **(f)** $\mathrm{Im}\left\{\mathrm{CFDAC}_{h^{(\mathrm{B8\text{-}1})},h^{(\mathrm{B8\text{-}3})}}\right\}$ **(g)** $\mathrm{Re}\left\{\mathrm{CFDAC}_{h^{(\mathrm{B8\text{-}1})},h^{(\mathrm{B8\text{-}4})}}\right\}$, **(h)** $\mathrm{Im}\left\{\mathrm{CFDAC}_{h^{(\mathrm{B8\text{-}1})},h^{(\mathrm{B8\text{-}4})}}\right\}$, **(i)** $\mathrm{Re}\left\{\mathrm{CFDAC}_{h^{(\mathrm{B8\text{-}1})},h^{(\mathrm{B8\text{-}5})}}\right\}$, **(j)** $\mathrm{Im}\left\{\mathrm{CFDAC}_{h^{(\mathrm{B8\text{-}1})},h^{(\mathrm{B8\text{-}5})}}\right\}$.

As expected, in Figure 4, the highest correlation corresponds to $\mathrm{CFDAC}_{h^{(\mathrm{B8\text{-}1})},h^{(\mathrm{B8\text{-}1})}}$, with the values symmetrically distributed along the main diagonal, since cymbal B8-1 is the pristine cymbal and is being correlated with itself. The next four comparisons with the pristine cymbal demonstrate small deviations from the main diagonal in the other CFDACs. These differences are expressed in terms of SCI in Figure 5. It is observed that the correlation between the real parts of the CFDACs is more prominent compared to that between the imaginary parts, leading to lower SCI values for the real parts. For the imaginary parts, the highest SCI value is 0.41, while for the real parts, it is 0.2. Additionally, the results in Figure 5 reveal that the highest correlation occurs between B8-1 and B8-5, indicating that these two cymbals exhibit similar vibrational behavior.
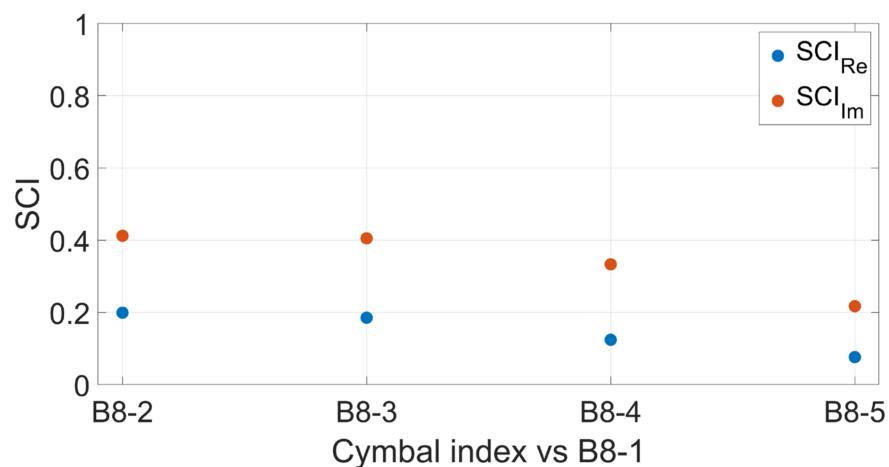
Figure 5. SCI calculated by comparing $\mathrm{CFDAC}_{h^{(\mathrm{B8\text{-}1})},h^{(\mathrm{B8\text{-}1})}}$ to $\mathrm{CFDAC}_{h^{(\mathrm{B8\text{-}1})},h^{(\mathrm{B8\text{-}2})}}$, $\mathrm{CFDAC}_{h^{(\mathrm{B8\text{-}1})},h^{(\mathrm{B8\text{-}3})}}$, $\mathrm{CFDAC}_{h^{(\mathrm{B8\text{-}1})},h^{(\mathrm{B8\text{-}4})}}$, and $\mathrm{CFDAC}_{h^{(\mathrm{B8\text{-}1})},h^{(\mathrm{B8\text{-}5})}}$. Blue: using the real parts of the CFDACs. Red: using the imaginary parts of the CFDACs.

The behavior of the CFDAC correlation values presents very small deviations, as expected, since the blank B8 group of cymbals is produced in the same factory using the same material and machining processes.

4.3. Correlation Between Blanks and Finished Cymbals

The B8-0 cymbal is the final product of a B8 blank cymbal, having passed through the remaining stages of the manufacturing process. Based on this, the correlation between the finished cymbal and the five blanks was calculated, providing $\text{CFDAC}_{h^{(\text{B8-0})}, h^{(\text{B8-1})}}$, $\text{CFDAC}_{h^{(\text{B8-0})}, h^{(\text{B8-2})}}$, $\text{CFDAC}_{h^{(\text{B8-0})}, h^{(\text{B8-3})}}$, $\text{CFDAC}_{h^{(\text{B8-0})}, h^{(\text{B8-4})}}$, and $\text{CFDAC}_{h^{(\text{B8-0})}, h^{(\text{B8-5})}}$. The real parts of the criteria are shown in Figure 6. As can be seen, the criterion values deviate from the main diagonal, with the lack of correlation becoming more pronounced after approximately 2 kHz. The differences in the FRFs can be attributed to the difference in mass between the finished and the blank cymbals, as well as the different number of processes the cymbals have undergone. The corresponding SCI values are depicted in Figure 7. The lowest values of SCI are associated with $\text{CFDAC}_{h^{(\text{B8-0})}, h^{(\text{B8-2})}}$ and $\text{CFDAC}_{h^{(\text{B8-0})}, h^{(\text{B8-3})}}$. As can be seen, these two CFDACs are less deviated from the main diagonal. Additionally, the lack of correlation between the vibrational behavior of the finalized and the blank cymbals results in SCI values above 0.4. By evaluating the vibrational behavior of all the blank cymbals considered in this section, it can be stated that the SCI values based on the real parts of the CFDACs lie between 0.4 and 0.6, while the values based on the imaginary parts range from 0.6 and 0.8. These values could serve as an indicator of the status of blank cymbals before entering the next manufacturing process.
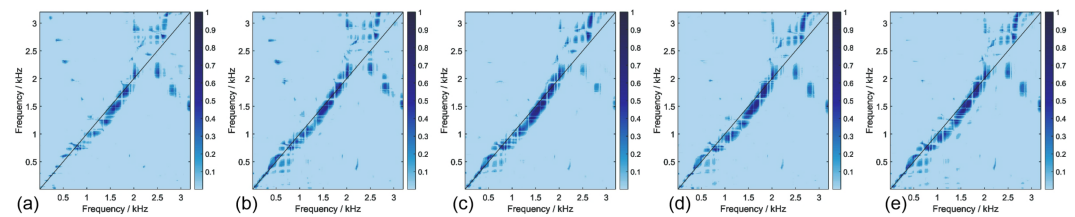
Figure 6. The real parts of the CFDACs between the finished B8 cymbal and the blank B8 cymbals. (**a**) $\text{Re}\left\{\text{CFDAC}_{h^{(\text{B8-0})}, h^{(\text{B8-1})}}\right\}$, (**b**) $\text{Re}\left\{\text{CFDAC}_{h^{(\text{B8-0})}, h^{(\text{B8-2})}}\right\}$, (**c**) $\text{Re}\left\{\text{CFDAC}_{h^{(\text{B8-0})}, h^{(\text{B8-3})}}\right\}$, (**d**) $\text{Re}\left\{\text{CFDAC}_{h^{(\text{B8-0})}, h^{(\text{B8-4})}}\right\}$, (**e**) $\text{Re}\left\{\text{CFDAC}_{h^{(\text{B8-0})}, h^{(\text{B8-5})}}\right\}$.
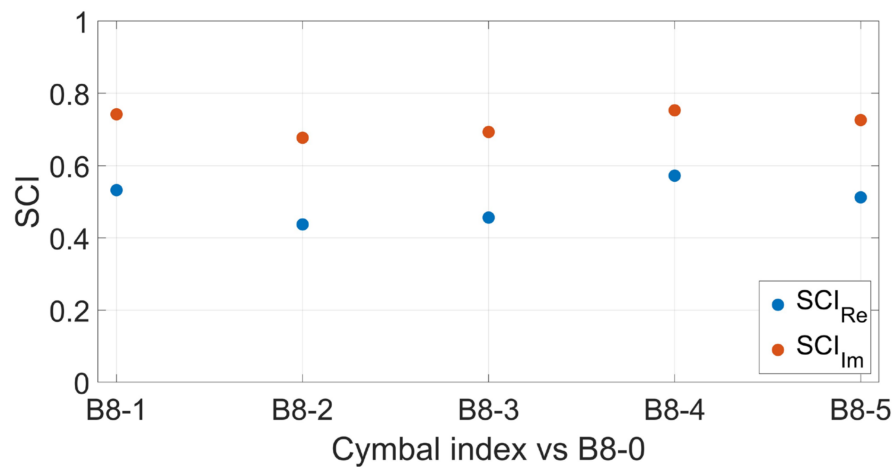
Figure 7. SCI calculated by comparing $\text{CFDAC}_{h^{(\text{B8-0})}, h^{(\text{B8-0})}}$ to $\text{CFDAC}_{h^{(\text{B8-0})}, h^{(\text{B8-1})}}$, $\text{CFDAC}_{h^{(\text{B8-0})}, h^{(\text{B8-2})}}$, $\text{CFDAC}_{h^{(\text{B8-0})}, h^{(\text{B8-3})}}$, $\text{CFDAC}_{h^{(\text{B8-0})}, h^{(\text{B8-4})}}$, and $\text{CFDAC}_{h^{(\text{B8-0})}, h^{(\text{B8-5})}}$. Blue: using the real parts of the CFDACs. Red: using the imaginary parts of the CFDACs.

The behavior of the CFDAC correlation values here indicates a variation along the main diagonal of the CFDAC graphs, since the finished B8-0 cymbal is compared to the blank B8 group of cymbals. Although B8-0 is a finished commercial cymbal, produced by a different manufacturer than the blanks, the common material and shape are recognized and reflected in the computed CFDAC values, as presented in Figures 6 and 7.

4.4. Correlation Between Blanks and Semi-Finished Cymbals

In this section, a comparison is performed between cymbals that have undergone two adjacent manufacturing stages. The FRFs of the blank B20 cymbals (B20-41, B20-42, B20-43, and B20-44) and the semi-finished cymbals (B20-51, B20-52, B20-53, B20-54, and B20-55) are used. The measurement data of B20-51 are used as the first set of the comparison. Initially, the real parts of all possible CFDACs, namely $\text{CFDAC}_{h^{(\text{B20-51})},h^{(\text{B20-41})}}$, $\text{CFDAC}_{h^{(\text{B20-51})},h^{(\text{B20-42})}}$, $\text{CFDAC}_{h^{(\text{B20-51})},h^{(\text{B20-43})}}$, $\text{CFDAC}_{h^{(\text{B20-51})},h^{(\text{B20-44})}}$, $\text{CFDAC}_{h^{(\text{B20-51})},h^{(\text{B20-51})}}$, $\text{CFDAC}_{h^{(\text{B20-51})},h^{(\text{B20-52})}}$, $\text{CFDAC}_{h^{(\text{B20-51})},h^{(\text{B20-53})}}$, $\text{CFDAC}_{h^{(\text{B20-51})},h^{(\text{B20-54})}}$, and $\text{CFDAC}_{h^{(\text{B20-51})},h^{(\text{B20-55})}}$, are shown in Figure 8.
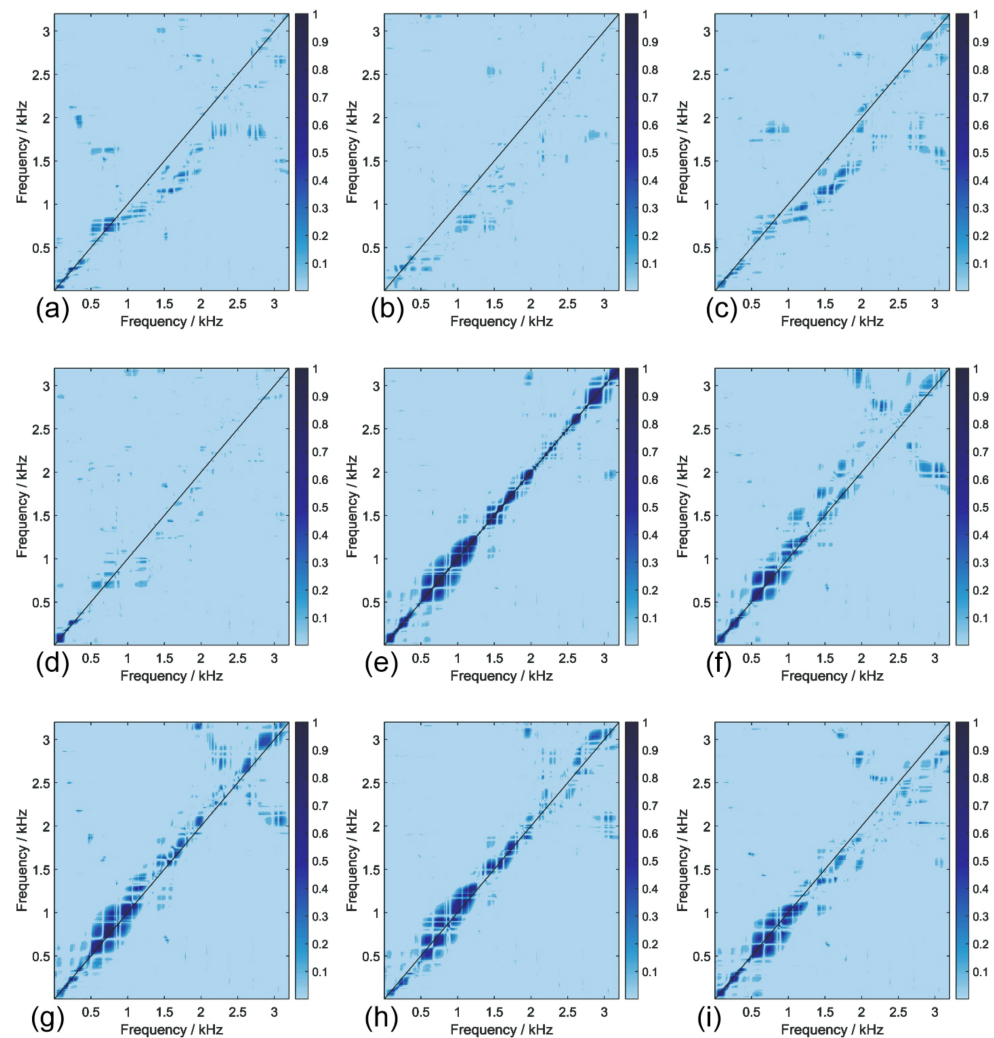
Figure 8. The real parts of the CFDACs between semi-finished B20-51 cymbal and the blank and semi-finished cymbals. (**a**) $\text{Re}\left\{\text{CFDAC}_{h^{(\text{B20-51})},h^{(\text{B20-41})}}\right\}$, (**b**) $\text{Re}\left\{\text{CFDAC}_{h^{(\text{B20-51})},h^{(\text{B20-42})}}\right\}$, (**c**) $\text{Re}\left\{\text{CFDAC}_{h^{(\text{B20-51})},h^{(\text{B20-43})}}\right\}$, (**d**) $\text{Re}\left\{\text{CFDAC}_{h^{(\text{B20-51})},h^{(\text{B20-44})}}\right\}$, (**e**) $\text{Re}\left\{\text{CFDAC}_{h^{(\text{B20-51})},h^{(\text{B20-51})}}\right\}$, (**f**) $\text{Re}\left\{\text{CFDAC}_{h^{(\text{B20-51})},h^{(\text{B20-52})}}\right\}$, (**g**) $\text{Re}\left\{\text{CFDAC}_{h^{(\text{B20-51})},h^{(\text{B20-53})}}\right\}$, (**h**) $\text{Re}\left\{\text{CFDAC}_{h^{(\text{B20-51})},h^{(\text{B20-54})}}\right\}$, (**i**) $\text{Re}\left\{\text{CFDAC}_{h^{(\text{B20-51})},h^{(\text{B20-55})}}\right\}$.

Figure 8 visualizes the lack of correlation between the FRFs of the semi-finished cymbal B20-51 and the blanks. The correlation increases when the B20-51 is compared to the other semi-finished cymbals. As expected, the highest correlation corresponds to $\text{CFDAC}_{h(\text{B20-51}),h(\text{B20-51})}$. It is also shown that the correlation between the reference cymbal and the other semi-finished cymbals is primarily concentrated at frequencies up to approximately 1.5 kHz.

It must be noted that in this case, the CFDAC visualizes the effect of hammering on the blank cymbals. Figure 9 presents the SCI values corresponding to the data shown in Figure 8. Observing Figure 9 enables a clear distinction between the blank and the semi-finished cymbals. Since hammering is not easily detectable through visual inspection, this observation is crucial for assessing the efficiency of the hammering process and verifying the production status of cymbals as semi-finished.
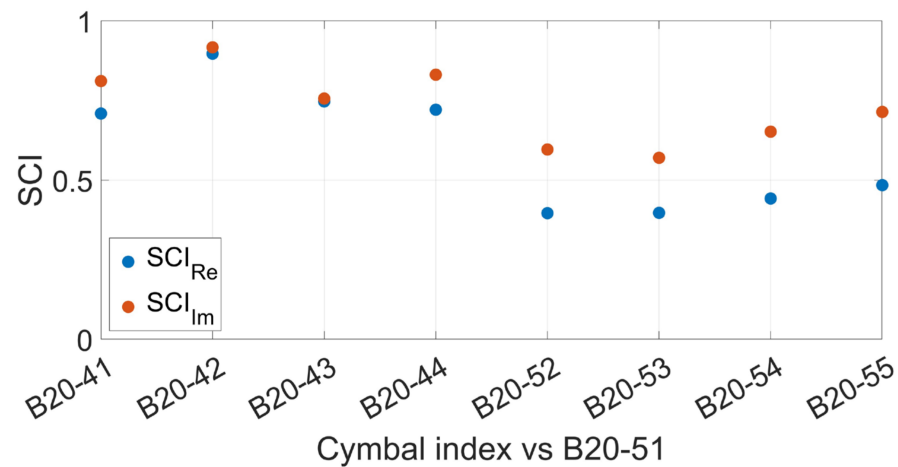
Figure 9. SCI calculated by comparing $\text{CFDAC}_{h(\text{B20-51}),h(\text{B20-51})}$ to $\text{CFDAC}_{h(\text{B20-51}),h(\text{B20-41})}$, $\text{CFDAC}_{h(\text{B20-51}),h(\text{B20-42})}$, $\text{CFDAC}_{h(\text{B20-51}),h(\text{B20-43})}$, $\text{CFDAC}_{h(\text{B20-51}),h(\text{B20-44})}$, $\text{CFDAC}_{h(\text{B20-51}),h(\text{B20-52})}$, $\text{CFDAC}_{h(\text{B20-51}),h(\text{B20-53})}$, $\text{CFDAC}_{h(\text{B20-51}),h(\text{B20-54})}$, and $\text{CFDAC}_{h(\text{B20-51}),h(\text{B20-55})}$. Blue: using the real parts of the CFDACs. Red: using the imaginary parts of the CFDACs.

4.5. Correlation Between Blanks and Finished Cymbals and Between Semi-Finished and Finished Cymbals

The differences in FRFs between the blank cymbals (B20-41, B20-42, B20-43, and B20-44) and each finished commercial cymbal (B20-1, B20-2, and B20-3) are investigated here. Additionally, a comparison is made between the semi-finished hammered cymbals (B20-51, B20-52, B20-53, B20-54, and B20-55) and the commercial cymbals. Figure 10 presents the real parts of the CFDACs, calculated using the B20-1 cymbal as the reference cymbal and the blank and semi-finished cymbals as the second cymbals in the comparisons (e.g., $\text{CFDAC}_{h(\text{B20-1}),h(\text{B20-41})}$).

As Figure 10 shows, the blank cymbals exhibit a lower correlation with the finished cymbals compared to the semi-finished cymbals. This is reflected in the lower CFDAC values for the blank cymbals in comparison to the semi-finished ones. Although the comparison between the finished and the semi-finished cymbals yields to higher CFDAC values, deviation from the main diagonal is observed, indicating that the FRFs being compared do not exhibit a high degree of similarity. Figure 11 shows all measured FRFs of the B20-1 cymbal, along with the FRFs of B20-42 and B20-52, for the frequency region between 100 Hz and 2 kHz. The graphs denote that the influence of hammering on the blank cymbals is evident in the separation of the resonant frequencies. This process causes the FRFs of the semi-finished cymbals to exhibit quantitative similarities to the FRFs of the finished cymbals.
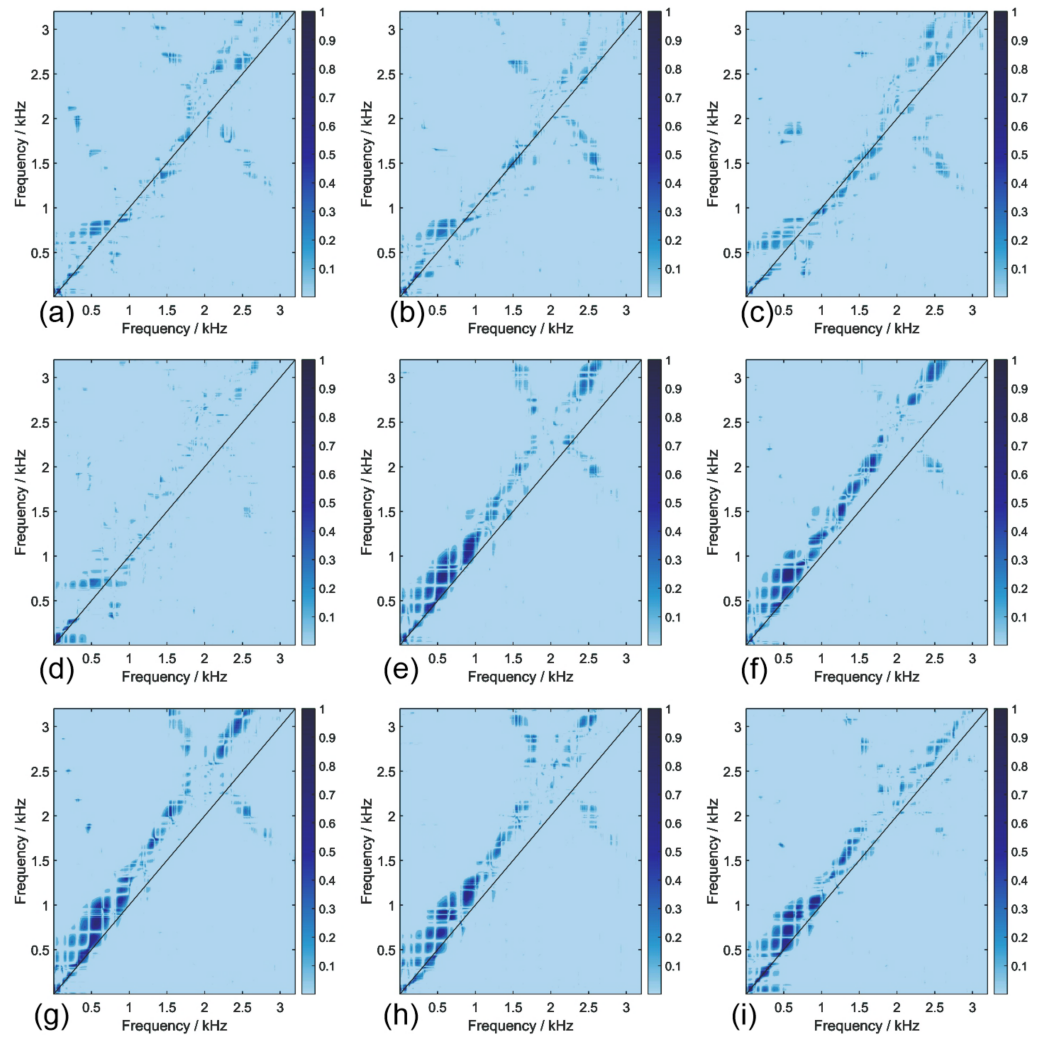
Figure 10. Real parts of CFDACs between the finished B20-1 cymbal and the blank and semi-finished B20 cymbals. (**a**) $\mathrm{Re}\left\{\mathrm{CFDAC}_{h^{(B20\text{-}1)},h^{(B20\text{-}41)}}\right\}$, (**b**) $\mathrm{Re}\left\{\mathrm{CFDAC}_{h^{(B20\text{-}1)},h^{(B20\text{-}42)}}\right\}$, (**c**) $\mathrm{Re}\left\{\mathrm{CFDAC}_{h^{(B20\text{-}1)},h^{(B20\text{-}43)}}\right\}$, (**d**) $\mathrm{Re}\left\{\mathrm{CFDAC}_{h^{(B20\text{-}1)},h^{(B20\text{-}44)}}\right\}$, (**e**) $\mathrm{Re}\left\{\mathrm{CFDAC}_{h^{(B20\text{-}1)},h^{(B20\text{-}51)}}\right\}$, (**f**) $\mathrm{Re}\left\{\mathrm{CFDAC}_{h^{(B20\text{-}1)},h^{(B20\text{-}52)}}\right\}$, (**g**) $\mathrm{Re}\left\{\mathrm{CFDAC}_{h^{(B20\text{-}1)},h^{(B20\text{-}53)}}\right\}$, (**h**) $\mathrm{Re}\left\{\mathrm{CFDAC}_{h^{(B20\text{-}1)},h^{(B20\text{-}54)}}\right\}$, (**i**) $\mathrm{Re}\left\{\mathrm{CFDAC}_{h^{(B20\text{-}1)},h^{(B20\text{-}55)}}\right\}$.
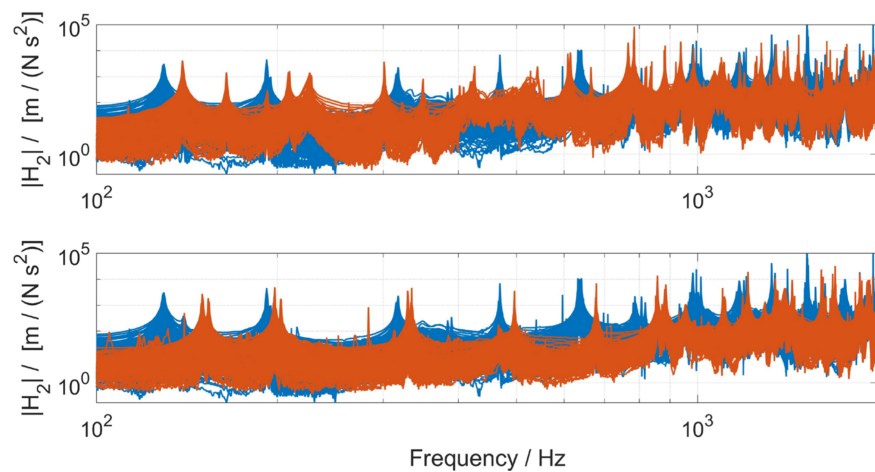
Figure 11. Magnitude of the FRFs of the BS20-1 finished cymbal (blue), B20-42 blank cymbal (red, top), and B20-52 semi-finished cymbal (red, bottom) vs. frequency.

Following the analysis of the previously presented correlations, the SCI was calculated for all possible CFDAC pairs, using all finished cymbals. All SCI values (real and imaginary) for these pairs are shown in Figure 12. The high SCI values across all pairs indicate that after the hammering stage, the semi-finished cymbals require additional processes to achieve vibrational characteristics comparable to those of the finished commercial cymbals. This qualitative representation of the cymbals' vibrational state is easily recognizable and may be used as a monitoring diagnostic tool for manufacturers and players. A hammered finished cymbal can be used as a sound reference to guide further machining of the semi-finished cymbal or to finalize the manufacturing process.
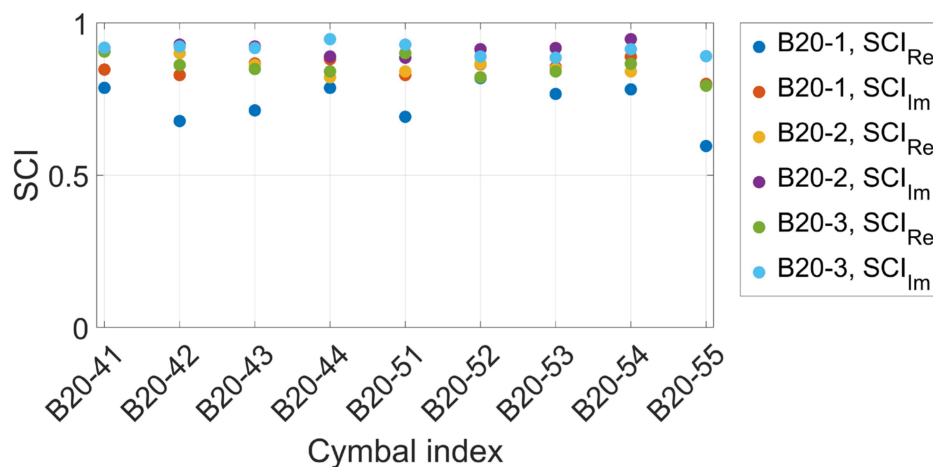
Figure 12. SCI calculated by using the CFDACs of the finished B20 cymbals and the CFDACs of the blank and semi-finished B20 cymbals.

4.6. Vibration Symmetry of Cymbals

The manufacturing processes up to the finishing stage introduce inhomogeneities to the volumetric shape of cymbals, which affects their vibrational behavior without influencing their circular axisymmetric macro-geometry. The degree of inhomogeneity can be quantified using CFDAC analysis followed by the SCI calculation. This calculation refers to changes in the SCI value resulting from changes in the sequence of the measured FRFs considered. Moreover, the SCI is based on comparisons of CFDAC matrices that contain the same data arranged in different rows. Specifically, 144 measured FRFs constitute the first CFDAC matrix, with rows indexed according to the measurement procedure (e.g., row 1 contains measurement point 1 data). For the second CFDAC matrix, the measurement data are reordered. Firstly, the data are shifted by 36 rows (a quarter of the total measurements). This means rows 1–108 of the new CFDAC matrix contain data for measurement points 37–144, while rows 109–144 contain data for measurement points 1–36. Secondly, the data are shifted by half of the total number of rows. Thus, rows 1–72 of the new CFDAC matrix contain data for measurement points 73–144, and rows 73–144 contain data for measurement points 1–72. The analysis was performed for the blank B8 cymbals (B8-1, B8-2, B8-3, B8-4, and B8-5) and the finished cymbals (MS63, B8-0, B20-1, B20-2, and B20-3). Figure 13 shows the SCI values when the originally measured data are compared to data shifted by 36 positions (marked as quarter shift—Q) and data shifted by 72 positions (marked as half shift—H). As observed, the quarter shift results in higher SCI values than the half shift. The change in the SCI values, when comparing the quarter shift to the half shift for the same cymbal data, indicates that in the case of the blank B8 cymbals, the data along the measurement diagonals are similar to a greater extent than in the case of the finalized cymbals. For the latter (MS63, B8-0, B20-1, B20-2, and B20-3), the smaller differences in SCI values suggest a greater degree of inhomogeneity, which

can be attributed to the processes undertaken after the blank stage. This finding reinforces the potential of using the SCI as a metric to quantify the changes in overall cymbal shape required by each manufacturer.
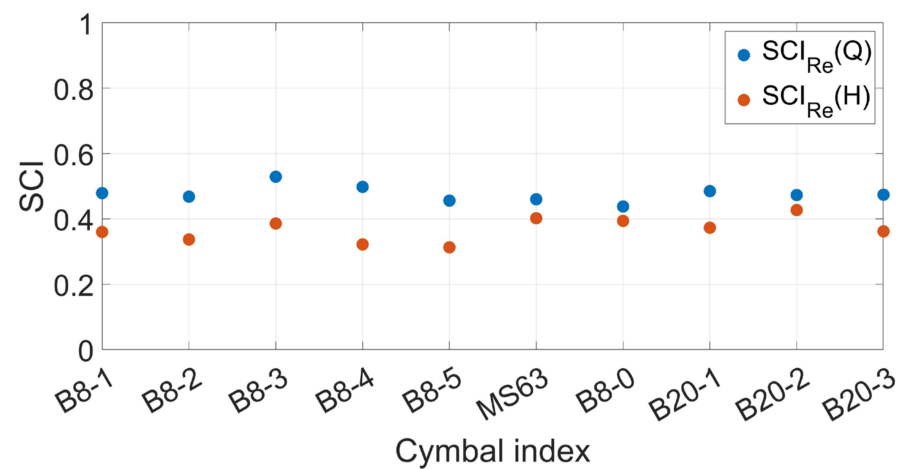
Figure 13. SCI calculated by using the CFDACs of the originally measured FRF matrix and the CFDACs after shifting the rows of the matrix.

5. Conclusions

This study explored the potential use of the CFDAC and the spectral correlation index in the cymbal manufacturing process. The proposed methodology highlights the influence of the manufacturing processes of forming, hammering, and finishing to the vibrational behavior of the cymbals and demonstrates the capability of the correlation criterion to monitor, identify, and visualize the vibrational state of any cymbal compared to a pristine one. Very small deviations in the criterion were observed for the blank cymbals, produced by the same manufacturer, using the same material and machining processes. Common materials and shapes were recognized and reflected in the computed values when comparing the hammered cymbals to a finished commercial cymbal. The CFDAC allows for a clear distinction between blanks and semi-finished cymbals, and since hammering cannot be easily visually detected, the proposed methodology offers a monitoring diagnostic tool capable of identifying the vibroacoustic state of a cymbal. The SCI values allow for the evaluation of the vibrational state of the cymbals and indicate if additional processes are required to lead the vibrational characteristics of the cymbal to a different state relative to a pristine reference. Additionally, the SCI was employed to evaluate the similarity of the FRFs within the same cymbal.

A qualitative representation of the cymbals' vibrational state was easily recognized, enabling a novel methodology for manufacturers and musicians to emerge. This offers a potential control tool for various stages of cymbal manufacturing. Moreover, in the context of automated cymbal measurements, this method offers a practical approach for use on production lines. A proposal for future research involves applying this method during the hammering process in incremental steps, enabling the tracking of changes in a cymbal's vibrational response after a predefined number of hammer hits. Additionally, extending this study to examine the behavior of non-finished cymbals in subsequent manufacturing stages will further enhance the knowledge and capability for sound emission prediction studies.

References

1. Rossing, T.D. *Science of Percussion Instruments*, 1st ed.; World Scientific: Singapore, 2000.
2. Perrin, R.; Swallowe, G.M.; Moore, T.R.; Zietlow, S.A. Normal modes of an 18 inch crash cymbal. *Proc. Inst. Acoust.* **2006**, *28 Pt 1*, 653–662.
3. Bucur, V. Struck Idiophones Played with Mallets: Gongs, Cymbals, Chimes, Sound Plates, Triangle. In *Handbook of Materials for Percussion Musical Instruments*; Springer: Cham, Switzerland, 2022; pp. 401–481.
4. Jossic, M.; Mamou-Mani, A.; Chomette, B.; Roze, D.; Ollivier, F.; Josserand, C. Modal active control of Chinese gongs. *J. Acoust. Soc. Am.* **2017**, *141*, 4567–4578. [CrossRef] [PubMed]
5. Fletcher, N.H.; Rossing, T.D. *Physics of Musical Instruments*, 2nd ed.; Springer: New York, NY, USA, 2010; pp. 640–674.
6. Schad, C.R.; Frik, G. Plattenglocken. *Acustica* **1996**, *82*, 158–168.
7. Bestle, P.; Hanss, M.; Eberhard, P. Experimental and numerical analysis of the musical behaviour of triangle instruments. In Proceedings of the 5th European Conference of Computational Mechanics (ECCM V), Barcelona, Spain, 20–25 July 2014; pp. 3104–3114.
8. Perrin, R.; Swallowe, G.M.; Zietlow, S.A.; Moore, T.R. The normal model of cymbals. *Proc. Inst. Acoust.* **2008**, *30 Pt 2*, 460–467.
9. Ducceschi, M.; Touzé, C. Modal approach for nonlinear vibrations of damped impacted plates: Application to sound synthesis of gongs and cymbals. *J. Sound Vib.* **2015**, *344*, 313–331. [CrossRef]
10. Chaigne, A.; Touzé, C.; Thomas, O. Mechanical models of musical instruments and sound synthesis: The case of gongs and cymbals. In Proceedings of the International Symposium on Musical Acoustics, Nara, Japan, 31 March–3 April 2004; hal-03179390.
11. Nguyen, Q.B.; Touzé, C. Nonlinear vibrations of thin plates with variable thickness: Application to sound synthesis of cymbals. *J. Acoust. Soc. Am.* **2019**, *145*, 977–988. [CrossRef] [PubMed]
12. Kaselouris, E.; Alexandraki, C.; Bakarezos, M.; Tatarakis, M.; Papadogiannis, N.A.; Dimitriou, V. A detailed FEM Study on the Vibro-acoustic Behaviour of Crash and Splash Musical Cymbals. *Int. J. Circuits Syst. Signal Process.* **2022**, *16*, 948–955. [CrossRef]
13. Brezas, S.; Kaselouris, E.; Orphanos, Y.; Tatarakis, M.; Bakarezos, M.; Papadogiannis, N.A.; Dimitriou, V. Vibrational Analysis of a Splash Cymbal by Experimental Measurements and Parametric CAD-FEM Simulations. *Vibration* **2024**, *7*, 146–160. [CrossRef]
14. Nakanishi, T.; Aihara, T.; Iwahar, M.; Sakai, T.; Minorikawa, G. Sound quality analysis of cymbals. In Proceedings of the INTER-NOISE15, San Fransisco, CA, USA, 9–12 August 2015; pp. 4353–4361.
15. Kaselouris, E.; Paschalidou, S.; Alexandraki, C.; Dimitriou, V. FEM-BEM Vibroacoustic Simulations of Motion Driven Cymbal-Drumstick Interactions. *Acoustics* **2023**, *5*, 165–176. [CrossRef]
16. Osamura, K.; Kuratani, F.; Koide, T.; Ogawa, W.; Taniguchi, H.; Monju, Y.; Mizuta, T.; Shobu, T. The correlation between the percussive sound and the residual stress/strain distributions in a cymbal. *J. Mater. Eng. Perform.* **2016**, *25*, 5323–5329. [CrossRef]
17. Cymbal Wiki. Available online: https://www.cymbal.wiki/wiki/Main_Page (accessed on 13 November 2024).
18. Kuratani, F.; Yoshida, T.; Koide, T.; Mizuta, T.; Osamura, K. Understanding the effect of hammering process on the vibration characteristics of cymbals. *J. Phys. Conf. Ser.* **2016**, *744*, 012110. [CrossRef]
19. Zildjian FX Raw Crash Small Bell. Available online: https://www.thomann.de/gr/zildjian_fx_raw_crash_small_bell.htm?glp=1&gad_source=1 (accessed on 17 January 2025).
20. Meinl. Byzance Vintage Cymbals. Available online: https://meinlcymbals.com/en/cymbals/ByzanceVintage (accessed on 17 January 2025).

21.	Pérez, M.A.; Serra-López, R. A frequency domain-based correlation approach for structural assessment and damage identification. *Mech. Syst. Signal Process.* **2019**, *119*, 432–456. [CrossRef]

22.	Pérez, M.A.; Font-Moré, J.; Fernández-Esmerats, J. Structural damage assessment in lattice towers based on a novel frequency domain-based correlation approach. *Eng. Struct.* **2021**, *226*, 111329. [CrossRef]

23.	Viala, R.; Pérez, M.A.; Placet, V.; Manjón, A.; Foltête, E.; Cogan, S. Towards model-based approaches for musical instruments making: Validation of the model of a Spanish guitar soundboard and characterization features proposal. *Appl. Acoust.* **2021**, *172*, 107591. [CrossRef]

24.	Giro, Y.; Le Carrou, J.L.; Vincenti, A.; Dartois, S.; Viala, R.; Navarret, B. Predicting the effects of bracing pattern modifications on acoustic guitar soundboards. In Proceedings of the Forum Acusticum, Turin, Italy, 11–15 September 2023; pp. 3419–3422.

25.	Brezas, S.; Kaselouris, E.; Grigoriou, D.; Papadaki, H.; Orphanos, Y.; Bakarezos, M.; Papadogiannis, N.A.; Dimitriou, V. Vibration analysis of 3D printed cymbals and Tzouras top plates. In Proceedings of the INTER-NOISE24, Nantes, France, 25–29 August 2024; pp. 6741–6749.

26.	Pérez, M.A.; Pernas-Sánchez, J.; Artero-Guerrero, J.A.; Serra-López, R. High-velocity ice impact damage quantification in composite laminates using a frequency domain-based correlation. *Mech. Syst. Signal Process.* **2021**, *147*, 107124. [CrossRef]

27.	Product Specifications. Available online: https://www.pcb.com/contentStore/docs/pcb_corporate/vibration/products/specsheets/086e80_c.pdf (accessed on 17 January 2025).

28.	Product Specifications. Available online: https://www.pcb.com/contentStore/docs/pcb_corporate/vibration/products/specsheets/tld352a56_e.pdf (accessed on 17 January 2025).

29.	Mc Connell, K.G.; Varoto, P.S. *Vibration Testing: Theory and Practice*; John Wiley & Sons: New York, NY, USA, 2008.